Transient Dynamics of Terrestrial Carbon Storage: Mathematical foundation and its applications

Yiqi Luo[1,2], Zheng Shi[1], Xingjie Lu[3], Jianyang Xia[4], Junyi Liang[1], Jiang Jiang[1], Ying Wang[5], Matthew J. Smith[6], Lifen Jiang[1], Anders Ahlström[7, 8], Benito Chen[9], Oleksandra Hararuk[10], Alan Hastings[11], Forrest Hoffman[12], Belinda Medlyn[13], Shuli Niu[14], Martin Rasmussen[15], Katherine Todd-Brown[16], Ying-Ping Wang[3]

[1]Department of Microbiology and Plant Biology, University of Oklahoma, Norman, Oklahoma, USA, [2]Center for Earth System Science, Tsinghua University, Beijing, China, [3]CSIRO Oceans and Atmosphere, Aspendale, Victoria, Australia, [4]School of Ecological and Environmental Sciences, East China Normal University, Shanghai, China, [5]Department of Mathematics, University of Oklahoma, Norman, Oklahoma, USA, [6]Computational Science Laboratory, Microsoft Research, Cambridge, UK, [7]Department of Earth System Science, Stanford University, Stanford, California, USA, [8]Department of Physical Geography and Ecosystem Science, Lund University, Lund, Sweden, [9]Department of Mathematics, University of Texas, Arlington, TX, USA, [10]Department of Natural Resource Sciences, McGill University, Montreal,, Canada, [11]Department of Environmental Science and Policy, University of California, One Shields Avenue, Davis, CA 95616, USA, [12]Computational Earth Sciences Group, Oak Ridge National Laboratory, Oak Ridge, TN 37831, USA, [13]Hawkesbury Institute for the Environment, Western Sydney University, Penrith NSW 2751, Australia, [14]Institute of Geographic Sciences and Natural Resources Research, Chinese Academy of Sciences, China, [15]Department of Mathematics, Imperial College, London, UK, [16]Biological Sciences Division, Pacific Northwest

24   National Laboratory, Richland, Washington, USA,

25

26

27   **Running Title**: Land carbon storage dynamics

28

29   **Correspondence author**: Yiqi Luo

30   Email: yluo@ou.edu

31   **Key words** Carbon cycle, carbon sequestration, dynamic disequilibrium, model intercomparison,

32   terrestrial ecosystems, traceability analysis

33   **Type of paper**: Primary Research Article

34

35

36   **Abstract** Terrestrial ecosystems have absorbed roughly 30% of anthropogenic CO_2 emissions

37   over the past decades, but it is unclear whether this carbon (C) sink will endure into the future.

38   Despite extensive modeling, experimental, and observational studies, what fundamentally

39   determines transient dynamics of terrestrial C storage under global change is still not very clear.

40   Here we develop a new framework for understanding transient dynamics of terrestrial C storage

41   through mathematical analysis and numerical experiments. Our analysis indicates that the

42   ultimate force driving ecosystem C storage change is the C storage capacity, which is jointly

43   determined by ecosystem C input (e.g., net primary production, NPP) and residence time. Since

44   both C input and residence time vary with time, the C storage capacity is time-dependent and

45   acts as a moving attractor that actual C storage chases. The rate of change in C storage is

46   proportional to the C storage potential, the difference between the current storage and the storage

47   capacity. The C storage capacity represents instantaneous responses of the land C cycle to

48   external forcing, whereas the C storage potential represents the internal capability of the land C

49   cycle to influence the C change trajectory in the next time step. The influence happens through

50   redistribution of net C pool changes in a network of pools with different residence times.

51   Moreover, this and our other studies have demonstrated that one matrix equation can

52   replicate simulations of most land C cycle models (i.e., physical emulators). As a result,

53   simulation outputs of those models can be placed into a three-dimensional (3D) parameter space

54   to measure their differences. The latter can be decomposed into traceable components to track

55   the origins of model uncertainty. In addition, the physical emulators make data assimilation

56   computationally feasible so that both C flux- and pool-related datasets can be used to better

57   constrain model predictions of land C sequestration. Overall, this new mathematical framework

58   offers new approaches to understand, evaluate, diagnose, and improve land C cycle models.

1 Introduction

Terrestrial ecosystems have been estimated to sequester approximately 30% of anthropogenic

carbon (C) emission in the past three decades (Canadell et al., 2007). Cumulatively, land

ecosystems have sequestered more than 160 Gt C from 1750 to 2015 (Le Quéré et al., 2015).

Without land C sequestration, the atmospheric CO_2 concentration would have increased by

additional 95 parts per million and result in more climate warming (Le Quéré et al., 2015).

During one decade from 2005 to 2014, terrestrial ecosystems sequestrated 3±0.8 Gt C per year

(Le Quéré et al., 2015), which would cost billion dollars if the equivalent amount of C was

sequestrated using C capture and storage techniques (Smith et al., 2016). Thus, terrestrial

ecosystems effectively mitigate global change through natural processes with minimal cost.

Whether this terrestrial C sequestration would endure into the future, however, is not clear,

making the mitigation of global change greatly uncertain. To predict future trajectories of C

sequestration in the terrestrial ecosystems, it is essential to understand fundamental mechanisms

that drive terrestrial C storage dynamics.

To predict future land C sequestration, the modeling community has developed many C

cycle models. According to a review by Manzoni and Porporato (2009), approximately 250

biogeochemical models have been published over a time span of 80 years to describe carbon and

nitrogen mineralization. The majority of those 250 models follow some mathematical

formulations of ordinary differential equations. Moreover, many of those biogeochemical models

incorporate more and more processes in an attempt to simulate C cycle processes as realistically

as possible (Oleson et al., 2013). As a consequence, terrestrial C cycle models have become

increasingly complicated and less tractable. Almost all model intercomparison projects (MIPs),

including those involved in the last three IPCC assessments, indicate that C cycle models have

82   consistently projected widely spread trajectories of land C sinks and were also found to fit

83   observations poorly (Todd-Brown et al., 2013; Luo et al., 2015). The lack of progress in

84   uncertainty analysis urges us to understand mathematical foundation of those terrestrial C models

85   so as to diagnose causes of model spreads and improve model predictive skills.

86   Meanwhile, many countries have made great investments on various observational and

87   experimental networks (or platforms) in hope to quantify terrestrial C sequestration. For

88   example, FLUXNET has been established about 20 years ago to quantify net ecosystem

89   exchange (NEE) between the atmosphere and biosphere (Baldocchi et al., 2001). Orbiting

90   Carbon Observatory 2 (OCO-2) satellite was launched in 2014 to quantify carbon dioxide

91   concentrations and distributions in the atmosphere at high spatiotemporal resolution to constrain

92   land surface C sequestration (Hammerling et al., 2012). Networks of global change experiments

93   have been designed to uncover processes that regulate ecosystem C sequestration (Rustad et al.,

94   2001; Luo et al., 2011; Fraser et al., 2013; Borer et al., 2014). Massive data have been generated

95   from those observational systems and experimental networks. They offer an unprecedented

96   opportunity for advancing our understanding of ecosystem processes and constraining model

97   prediction of ecosystem C sequestration. Indeed, many of those networks were initiated with one

98   goal to improve our predictive capability. Yet the massive data have been rarely integrated into

99   earth system models to constrain their predictions. It is a grand challenge in our era to develop

100   innovative approaches to integration of big data into complex models so as to improve prediction

101   of future ecosystem C sequestration.

102   From a system perspective, ecosystem C sequestration occurs only when the terrestrial C

103   cycle is in a transient state, under which C influx into one ecosystem is larger than C efflux from

104   the ecosystem. Olson (1963) is probably among the first to examine organic matter storage in

105   forest floors from the system perspective. His analysis approximated steady-state storage of

106   organic matter as a balance of litter producers and decomposers for different forest types.

107   However, global change differentially influences various C cycle processes in ecosystems and

108   results in transient dynamics of terrestrial C storage (Luo and Weng, 2011). For example, rising

109   atmospheric CO_2 concentration primarily stimulates photosynthetic C uptake while climate

110   warming likely enhances decomposition. When ecosystem C uptake increases in a unidirectional

111   trend under elevated $[CO_2]$, terrestrial C cycle is at disequilibrium, leading to net C storage. The

112   net gained C is first distributed to different pools, each of which has a different turnover rate (or

113   residence time) before C is eventually released back to the atmosphere via respiration.

114   Distribution of net C exchange to multiple pools with different residence times is an intrinsic

115   property of an ecosystem to gradually equalize C efflux with influx (i.e. internal recovery force

116   toward an attractor). In contrast, global change factors that causes changes in C input and

117   decomposition is considered external forces that create disequilibrium through altering internal C

118   processes and pool sizes. The transient dynamics of terrestrial C cycle at disequilibrium is

119   maintained by interactions of internal processes and external forces (Luo and Weng, 2011).

120   Although the transient dynamics of terrestrial C storage have been conceptually discussed, we

121   still lack a quantitative formulation to estimate transient C storage dynamics in the terrestrial

122   ecosystems.

123   This paper was designed to address a question: what determines transient dynamics of C

124   storage in terrestrial ecosystems from a system perspective? We first reviewed the major

125   processes that most models have incorporated to simulate terrestrial C sequestration. The review

126   helps establish that terrestrial C cycle can be mathematically represented by a matrix equation.

127   We also described the Terrestrial ECOsystem (TECO) model with its numerical experiments in

128 support of the mathematical analysis. We then presented results of mathematical analysis on

129 determinants of the terrestrial C storage, direction and magnitude of C storage at a given time

130 point, and numerical experiments to illustrate climate impacts on terrestrial C storage. We

131 carefully discussed assumptions of those terrestrial C cycle models as represented by the matrix

132 equation, the validity of this analysis, and two new concepts introduced in this study, which are

133 the C storage capacity and C storage potential. We also discussed the potential applications of

134 this analysis to model uncertainty analysis and data-model integration. Moreover, we proposed

135 that the C storage potential be a targeted variable for research, trading, and government

136 negotiation for C credit.

137

138 **2 Methods**

139 **2.1 Mathematical representation of terrestrial C cycle**

140 This study was conducted mainly with mathematical analysis. We first established the basis of

141 this analysis, which is that the majority of terrestrial C cycle models can be represented by a

142 matrix equation.

143   Hundreds of models have been developed to simulate terrestrial C cycle (Manzoni and

144 Porporato, 2009). All the models have to simulate processes of photosynthetic C input, C

145 allocation and transformation, and respiratory C loss. It is well understood that photosynthesis is

146 a primary pathway of C flow into land ecosystems. Photosynthetic C input is usually simulated

147 according to carboxylation and electron transport rates (Farquhar et al., 1980). Ecosystem C

148 influx varies with time and space mainly due to variations in leaf photosynthetic capacity, leaf

149 area index of canopy, and a suite of environmental factors such as temperature, radiation, and

150 relative humidity (or other water-related variables) (Potter et al., 1993; Sellers et al., 1996;

151   Keenan et al., 2012; Walker et al., 2014, Parolari and Porporato 2016).

152   Photosynthetically assimilated C is partly used for plant biomass growth and partly

153   released back into the atmosphere through plant respiration. Plant biomass in leaves and fine

154   roots usually lives for several months up to a few years before death, while woody tissues may

155   persist for hundreds of years in forests. Dead plant materials are transferred to litter pools and

156   decomposed by microorganisms to be partially released through heterotrophic respiration and

157   partially stabilized to form soil organic matter (SOM). SOM can store C in the soil for hundreds

158   or thousands of years before it is broken down to CO_2 through microbial respiration (Luo and

159   Zhou, 2006). This series of C cycle processes has been represented in most ecosystem models

160   with multiple pools linked by C transfers among them (Jenkinson et al., 1987; Parton et al., 1987;

161   1988; 1993), including those embedded in Earth system models (Ciais et al., 2013).

162   The majority of the published 250 terrestrial C cycle models use ordinary differential

163   equations to describe C transformation processes among multiple plant, litter, and soil pools

164   (Manzoni and Porporato, 2009). Those ordinary differential equations can be summarized into a

165   matrix formula (Luo et al., 2001; 2003; Luo and Weng, 2011; Luo et al., 2015; 2016; Sierra and

166   Müller 2015) as:

167
$$\begin{cases} X'(t) = Bu(t) - A\xi(t)KX(t) \\ X(t = 0) = X_0 \end{cases} \qquad (1)$$

168   where $X'(t)$ is a vector of net C pool changes at time t, $X(t)$ is a vector of pool sizes, B is a

169   vector of partitioning coefficients from C input to each of the pools, $u(t)$ is C input rate, A is a

170   matrix of transfer coefficients (or microbial C use efficiency) to quantify C movement along the

171   pathways, K is a diagonal matrix of exit rates (mortality for plant pools and decomposition

172   coefficients of litter and soil pools) from donor pools, $\xi(t)$ is a diagonal matrix of environmental

173   scalars to represent responses of C cycle to changes in temperature, moisture, nutrients, litter

8

174   quality, and soil texture, and X_0 is a vector of initial values of pool sizes of X. In eq. 1, all the

175   off-diagonal elements of matrix A, a_{ji}, are negative to reverse the minus sign and indicate

176   positive C influx to the receiving pools. The equation describes net C pool change, $X'(t)$, as a

177   difference between C input, $u(t)$, distributed to different plant pools via partitioning coefficients,

178   B, and C loss through the C transformation matrix, $A\xi(t)K$, among individual pools, $X(t)$.

179   Elements in vector B, matrices A and K could vary with many factors, such as vegetation types,

180   soil texture, microbial attributes, and litter chemistry. For example, vegetation succession may

181   influence elements in vector B, matrices A and K in addition to C input, $u(t)$, and forcing that

182   affects C dynamics through environmental scalars, $\xi(t)$.

183   After synthesis of all the possible soil C cycle models based on six principles (mass

184   balance, substrate dependence of decomposition, heterogeneity of decay rates, internal

185   transformations of organic matter, environmental variability effects, and substrate interactions),

186   Sierra and Müller (2015) concluded that this form of matrix equation such as eq. 1 represents the

187   majority of terrestrial C cycle models. Similarly, Manzoni and Porporato (2009) concluded their

188   review of 250 models that the majority of them use ordinary differential equations, which can be

189   summarized by eq. 1, to describe land C cycle. Our mathematical analysis in this study used

190   matrix operations of eq. 1 to reveal determinants of transient dynamics of terrestrial C cycle,

191   including direction and rate of C storage changes, in response to global change. We examined

192   assumptions underlying this equation and the validity of our analysis in the Discussion section.

193

194   **2.2 TECO Model, its physical emulator, and numerical experiments**

195   We conducted numerical experiments to support the mathematical analysis and thus help

196   understand the characteristics of terrestrial C storage dynamics using the Terrestrial ECOsystem

197   (TECO) model. TECO has five major components: canopy photosynthesis, soil water dynamics,

198   plant growth, litter and soil carbon decomposition and transformation, and nitrogen dynamics as

199   described in detail by Weng and Luo (2008) and Shi et al. (2016). Canopy photosynthesis is

200   referred from a two-leaf (sunlit and shaded) model developed by Wang and Leuning (1998). This

201   submodel simulates canopy conductance, photosynthesis, and partitioning of available energy.

202   The model combines the leaf photosynthesis model developed by Farquhar et al. (1980) and a

203   stomatal conductance model (Harley et al., 1992). In the soil water dynamic submodel, soil is

204   divided into 10 layers. The surface layer is 10 cm deep and the other 9 layers are 20 cm deep.

205   Soil water content (SWC) in each layer results from the mass balance between water influx and

206   efflux. The plant growth submodel simulates C allocation and phenology. Allocation of C among

207   three plant pools, which are leaf, fine root, and wood, depends on their growth rates (Fig. 1a).

208   Phenology dynamics is related to leaf onset, which is triggered by growing degree days, and leaf

209   senescence, which is determined by temperature and soil moisture. The C transformation

210   submodel estimates carbon transfer from plants to two litter pools and three soil pools (Fig. 1a).

211   The nitrogen (N) submodel is fully coupled with C processes with one additional mineral N pool.

212   Nitrogen is absorbed by plants from mineral soil and then partitioned among leaf, woody tissues

213   and fine roots. Nitrogen in plant detritus is transferred among different ecosystem pools (i.e.

214   litter, coarse wood debris, fast, slow and passive SOM) (Shi et al., 2016). The model is driven by

215   climate data, which include air and soil temperature, vapor-pressure deficit, relative humidity,

216   incident photosynthetically active radiation, and precipitation at hourly steps.

217   We first calibrated TECO with eddy flux data collected at Harvard Forest from 2006-

218   2009. The calibrated model was spun up to the equilibrium state in pre-industrial environmental

219   conditions by recycling a 10-year climate forcing (1850-1859). Then the model was used to

220   simulate C dynamics from year 1850 to 2100 with the historical forcing scenario for 1850-2005

221   and RCP8.5 scenario for 2006-2100 as in the Community Land Model 4.5 (Oleson et al., 2013)

222   in the grid cell where Harvard Forest is located.

223   To support the mathematical analysis using eq. 1, we first developed a physical emulator

224   (i.e., the matrix representation of eq. 1) of the TECO model and then verified that the physical

225   emulator can closely represent simulations of the original TECO model. We first identified those

226   parameter values in each of the C balance equations in the TECO model that are corresponding

227   to elements in matrices A and K in eq. 1. The time-dependent variables for $u(t)$, elements in

228   vector B, and elements in matrix $\xi(t)$ in the physical emulator were directly from outputs of the

229   original TECO model. Then those parameter values and time-dependent variables were

230   organized into matrices A, $\xi(t)$, and K; vectors $X(t)$, X_0, and B; and variable $u(t)$. Note that

231   values of $u(t)$, B, and $\xi(t)$ could be different among different climate scenarios. Those matrices,

232   vectors, and variable were entered to matrix calculation to compute $X'(t)$ using eq. 1. The sum

233   of elements in calculated $X'(t)$ is a 100% match with simulated net ecosystem production (NEP)

234   with the TECO model (Fig. 1b).

235   Once eq. 1 was verified to exactly replicate TECO simulations, we used TECO to

236   generate numerical experiments to support the mathematical analysis on the transient dynamics

237   of terrestrial C storage. To analyze the seasonal patterns of C storage dynamics, we averaged 10

238   series of three-year seasonal dynamics from 1851-1880. Then we used a 7-day moving window

239   to further smooth the data.

240

241   **3. Results**

242

3.1 Determinants of C storage dynamics

243   **3.1 Determinants of C storage dynamics**

244   The transient dynamics of terrestrial carbon storage are determined by two components: the C

245   storage capacity and the C storage potential. The two components of C storage dynamics can be

246   mathematically derived from multiplying both sides of eq. 1 by $(A\xi(t)K)^{-1}$ as:

247            $X(t) = (A\xi(t)K)^{-1}Bu(t) - (A\xi(t)K)^{-1}X'(t)$ (2)

248   The first term on the right-hand side of eq. 2 is the C storage capacity and the second term is the

249   C storage potential. Fig. 2a shows time courses of C storage and its capacity over one year for

250   the leaf pool of Harvard Forest.

251   In eq. 2, we name the term $(A\xi(t)K)^{-1}$ the chasing time, $\tau_{ch}(t)$, with a time unit used in

252   exit rate K. The chasing time is defined as:

253            $\tau_{ch}(t) = (A\xi(t)K)^{-1}$ (3)

254     $\tau_{ch}(t)$ is a matrix of C residence times through the network of individual pools each with a

255   different residence time and fractions of received C connected by pathways of C transfer.

256   Analogous to the fundamental matrix measuring life expectancies in demographic models

257   (Caswell, 2000), the matrix, $\tau_{ch}(t)$, here measures expected residence time of a C atom in pool i

258   when it has entered from pool j. We call this matrix the fundamental matrix of chasing times to

259   represent the time scale at which the net C pool change, $X'(t)$, is redistributed in the network.

260   Meanwhile, the residence times of individual pools in network, $\tau_N(t)$, can be estimated by

261   multiplying the fundamental matrix of chasing times, $(A\xi(t)K)^{-1}$, with a vector of partitioning

262   coefficients, B as:

263            $\tau_N(t) = (A\xi(t)K)^{-1}B$ (4a)

264   Ecosystem residence time, $\tau_E(t)$, is the sum of the residence time of all individual pools in

265   network as:

266 $\tau_E(t) = (1 \quad 1 \quad \cdots \quad 1)\tau_N(t)$ (4b)

267 Thus, the C storage capacity can be defined by:

268 $X_c(t) = (A\xi(t)K)^{-1}Bu(t)$ (5a)

269 Alternatively, it can be estimated from C input, $u(t)$, and residence time, $\tau_N(t)$, as:

270 $X_C(t) = \tau_N(t)u(t)$ (5b)

271 As C input (e.g., Gross or Net Primary Productions, GPP or NPP) and residence times vary with

272 time, the C storage capacity varies with time. It represents instantaneous responses of the

273 terrestrial C cycle to the external forcing. The modeled C storage capacity in the leaf pool (Fig.

274 2a), for example, increases in spring, reaches the peak at summer, declines in autumn, and

275 becomes minimal in winter largely due to strong seasonal changes in C input (Fig. 2b). Note that

276 either GPP or NPP can be used as C input for analysis of transient C dynamics. Estimated

277 residence times, however, are smaller with GPP as C input than those with NPP as input. In this

278 paper, we mostly used NPP as C input as that fraction of C is distributed among pools.

279 The C storage potential at time t, $X_p(t)$, can be mathematically described as:

280 $X_p(t) = (A\xi(t)K)^{-1}X'(t)$ (6a)

281 Or it can be estimated from net C pool change, $X'(t)$, and chasing time, $\tau_{ch}(t)$ as:

282 $X_p(t) = \tau_{ch}(t)X'(t)$ (6b)

283 Eqs. 6a and 6b suggest that the C storage potential represents re-distribution of net C pool

284 change, $X'(t)$, of individual pools through a network of pools with different residence times as

285 connected by C transfers from one pool to the others through all the pathways. As time evolves,

286 the net C pool change, $X'(t)$, is redistributed again and again through the network of pools. The

287 network of redistribution of next C pool change, thus, represents the potential of an ecosystem to

288 store additional C when it is positive and lose C when it is negative. The C storage potential can

13

289   also be estimated from the difference between the C storage capacity and the C storage itself at

290   time t as:

291        $$X_p(t) = X_c(t) - X(t) \qquad\qquad\qquad (6c)$$

292   The C storage potential in the leaf pool, for example, is about zero in winter and early spring

293   when the C storage capacity is very close to the storage itself (Fig. 2a). The C storage potential is

294   positive when the capacity is larger than the storage itself from late spring to summer and early

295   fall. As the storage capacity decreases to the point when the storage equals the capacity on the

296   265th day of year (DOY), the C storage potential is zero. After that day, the C storage potential

297   becomes negative.

298   Dynamics of ecosystem C storage, $X(t)$, can be characterized by three parameters: C

299   influx, $u(t)$, residence times, $\tau_N(t)$, and the C storage potential $X_p(t)$ as:

300        $$X(t) = \tau_N(t)u(t) - X_p(t) \qquad\qquad\qquad (7)$$

301   Eq. 7 represents a three-dimensional (3D) parameter space within which model simulation

302   outputs can be placed to measure how and how much they diverge.

303   Note that sums of elements of vectors $X(t)$, $X_c(t)$, $X_p(t)$, and $X'(t)$ are corresponding,

304   respectively, to the whole ecosystem C stock, ecosystem C storage capacity, ecosystem C storage

305   potential, and net ecosystem production (NEP). In this paper, we describe them wherever

306   necessary rather than use a separate set of symbols to represent those sums.

307

308   **3.2 Direction and rate of C storage change at a given time**

309   Like studying any moving object, quantifying dynamics of land C storage needs to determine

310   both the direction and the rate of its change at a given time. To determine the direction and rate

311   of C storage change, we re-arranged eq. 2 to be:

14

312 $$\tau_{ch}X'(t) = X_c(t) - X(t) = X_p(t) \tag{8a}$$

313 or re-arranging eq. 6a leads to:

314 $$X'(t) = A\xi(t)KX_p(t) \tag{8b}$$

315 As all the elements in τ_{ch} are positive, the sign of $X'(t)$ is the same as for $X_p(t)$. That means

316 $X'(t)$ increases when $X_c(t) > X(t)$, does not change when $X_c(t) = X(t)$, and decreases when

317 $X_c(t) < X(t)$ at the ecosystem scale. Thus, the C storage capacity, $X_c(t)$, is an attractor and

318 hence determines the direction toward which the C storage, $X(t)$, chases at any given time point.

319 The rate of C storage change, $X'(t)$, is proportional to $X_p(t)$ and also regulated by τ_{ch}.

320 When we study C cycle dynamics, we are interested in understanding dynamics of not

321 only a whole ecosystem but also individual pools. Eq. 8a can be used to derive equations to

322 describe C storage change for an ith pool as:

323 $$\sum_{j=1}^{n} f_{ij}\,\tau_i\,x'_j(t) = \sum_{j=1}^{n} f_{ij}\,\tau_i b_j u(t) - x_i(t) = x_{p,i}(t) \tag{9a}$$

324 where n is the number of pools in a C cycle model, f_{ij} is a fraction of C transferred from pool j

325 to i through all the pathways, τ_i measures residence times of individual pools in isolation (in

326 contrast to τ_N in the network), x'_j is the net C change in the jth pool, b_j is a partitioning

327 coefficient of C input to the jth pool, $x_i(t)$ is the C storage in the ith pool, and $x_{p,i}(t)$ is the C

328 storage potential in the ith pool. Eq. 9a means that the C storage potential of each pool at time t,

329 $x_{p,i}(t)$, is the sum of all the individual net C pool change, x'_j, multiplied by corresponding

330 residence time spent in pool i coming from pool j. Through re-arrangement, eq. 9a can be solved

331 for each individual pool net C change as a function of C storage potential of all the pools as:

332 $$x'_i(t) = \frac{x_{c,i,u}(t) - x_{c,i,p}(t) - x_i(t)}{f_{ii}\tau_i} \tag{9b}$$

15

333 where $x_{c,i,u}(t) = \sum_{j=1}^{n} f_{ij} \tau_i b_j u(t)$ for the maximal amount of C that can transfer from C input

334 to the ith pool. $x_{c,i,p}(t) = \sum_{j=1, j \neq i}^{n} f_{ij} \tau_i x'_j(t)$ for the maximal amount of C that can transfer from

335 all the other pools to the ith pool. $f_{ii} = 1$ for all the pools if there is no feedback of C among soil

336 pools. $f_{ii} < 1$ when there are feedbacks of C among soil pools.

337   As plant pools get C only from photosynthetic C input, $u(t)$, but not from other pools,

338 the direction and rate of C storage change in the ith plant pool is determined by:

339
$$\begin{cases} x'_i(t) = \dfrac{x_{c,i}(t) - x_i(t)}{\tau_i} = \dfrac{X_{p,i}(t)}{\tau_i} \\ x_{c,i}(t) = b_i u(t) \tau_i \end{cases} \qquad \text{for } i = 1, 2, 3 \qquad (10)$$

340 The C storage capacity of plant pools equals the product of plant C input, $u(t)$ (i.e., net primary

341 production, NPP), partitioning coefficient, b_i, and residence time, τ_i, of its own pool (Fig. 2b-d).

342 Thus, the C storage capacities of the leaf, root, and wood pools are high in summer and low in

343 winter. Plant C storage, $x_i(t)$, still chases the storage capacity, $x_{c,i}(t)$, of its own pool at a rate

344 that is proportional to $X_{p,i}(t)$. For the leaf pool, the C storage, $x_1(t)$, increases when $x_{c,1}(t) >$

345 $x_1(t)$ (or $x_{p,1}(t) > 0$) from late spring until early fall on the 265th day of year (DOY) and then

346 decreases when $x_{c,1}(t) < x_1(t)$ (or $x_{p,1}(t) < 0$) from DOY of 265 until 326 during fall (Fig. 2a).

347   However, the direction of C storage change in litter and soil pools are no longer solely

348 determined by the storage capacity, $x_{c,i}(t)$, of their own pools or at a rate that is proportional to

349 $X_{p,i}(t)$. The C storage capacity of one litter or soil pool has two components. One component,

350 $x_{c,i,u}(t)$ is set by the amount of plant C input, $u(t)$, going through all the possible pathways,

351 $f_{ij}b_j$, multiplied by residence time, τ_i, of its own pool. The second component measures the C

352 exchange of one litter or soil pool with other pools according to net C pool change, $x'_j(t)$,

353 through pathways, $f_{ij}, j \neq i$, weighed by residence time, τ_i, of its own pool. For example, C

354 input to the litter pool is a combination of C transfer from C input through the leaf, root, and

16

355 wood pools (Fig. 3c, 3d, and 3e) and C transfer due to the net C pool changes in the leaf, root,

356 and wood pools (Fig. 3f, 3g, and 3h). Thus the first capacity component of the litter pool to store

357 C is the sum of three products of NPP, C partitioning coefficient, and network residence time,

358 respectively, through the leaf, root, and wood pools (Fig. 3c, 3d, and 3e). The second capacity

359 component is the sum of other three products of C transfer coefficient along all the possible

360 pathways, network residence time, and net C pool changes, respectively, in the leaf, root, and

361 wood pools (Fig. 3f, 3g, and 3h). Thus, C storage in the ith pool, $x_i(t)$, chases an attractor,

362 $(\sum_{j=1}^{n} f_{ij} b_j u(t) - \sum_{j=1,j\neq i}^{n} f_{ij} \tau_i x'_j(t))\tau_i$, for litter and soil pools (Fig. 4).

363   In summary, due to the network of C transfer, C storage in litter and soil pools does not

364 chase the C storage capacities of their own pools in a multiple C pool model (Fig. 4). The

365 capacities for individual litter and soil pools measure the amounts of C that is transferred from

366 photosynthetic C input through plant pools to be stored in those pools. However, those litter and

367 soil pools also exchange C with other pools according to transfer coefficients along pathways of

368 C movement multiplying net C pool change in those pools. Integration of the C input and C

369 exchanges together still sets as a moving attractor toward which individual pool C storage

370 approaches (Fig. 4).

371

372 **3.3 C storage dynamics under global change**

373 In response to a global change scenario that combines historical change and simulated RCP8.5 in

374 the TECO experiment, the modeled ecosystem C storage capacity (the sum of all elements in

375 vector $X_c(t)$) at Harvard Forest increases from 27 kg C m^{-2} in 1850 to approximately 38 kg C m^{-}

376 ^{2} in 2100 with strong interannual variability (Fig. 5a). The increasing capacity results from a

377 combination of a nearly 44% increase in NPP with a ~2% decrease in ecosystem residence times

17

378   (the sum of all elements in vector $\tau_E(t)$) during that period (Fig. 5b). The strong interannual

379   variability in the modeled capacity is attributable to the variability in NPP and residence times,

380   both of which directly respond to instantaneous variations in environmental factors. In

381   comparison, the ecosystem C storage (the sum of all elements in vector $X(t)$) itself gradually

382   increases, lagging behind the capacity, with much dampened interannual variability (Fig. 5a).

383   The dampened interannual variability is due to smoothing effects of pools with various residence

384   times. In response to global change scenario RCP8.5, the ecosystem C storage potential (the sum

385   of all elements in vector $X_p(t)$) in the Harvard Forest ecosystem increases from zero at 1980 to

386   3.5 kg C m^{-2} in 2100 with strong fluctuation over years (Fig. 5a). Over seasons, the potential is

387   high during the summer and low in winter, similarly with the seasonal cycle of the C storage

388   capacity.

389   Since chasing time, τ_{ch}, is a matrix and net C pool change, $X'(t)$, is a vector, eq. 6a or 6b

390   (i.e., the C storage potential) can not be analytically separated into the chasing time and net C

391   pool change as can the capacity into C input and residence time in eq. 5a or 5b for traceability

392   analysis. The relationships among the three quantities can be explored by regression analysis.

393   The ecosystem C storage potential fluctuates in a similar phase with NEP from 1850 to 2100

394   (Fig. 5c). Consequently, the C storage potential is well correlated with NEP at the whole

395   ecosystem scale (Fig. 5d). The slope of the regression line is a statistical representation of

396   ecosystem chasing time. In this study, we find that r^2 of the relationship between the storage

397   potential and NEP is 0.79. The regression slope is 28.1 years in comparison with the ecosystem

398   residence time of approximately 22 years (Fig. 5b).

399   The capacity and storage itself of individual pools display similar long-term trends and

400   interannual variability to those for the total ecosystem C storage dynamics (Fig. 6). Noticeably,

401   the deviation of the C storage from the capacity, which is the C storage potential, is much larger

402   for pools with long residence times than those with short residence times. For individual pools,

403   the potential is nearly zero for those fast turnover pools and becomes very large for those pools

404   with long residence time (Fig. 6).

405   For individual plant pools, eq. 10 describes the dependence of the C storage potential,

406     $x_{p,i}(t)$, on the pool-specific residence time, τ_i, $i = 1, 2,$ and 3, and net C pool change of their

407   own pools, $x'_i(t)$, $i = 1, 2,$ and 3. Thus, one value of $x_{p,i}(t)$ is exactly corresponding to one

408   value of $x'_i(t)$ at slope of τ_i, leading to the correlation coefficient in Fig. 7 being 1.00 for leaf,

409   root, and wood pools. For a litter or soil pool, however, the C storage potential is not solely

410   dependent on the residence time and net C pool change of its own pool but influenced by several

411   other pools. Thus, the potential of one litter or soil pool is correlated with net C pool changes of

412   several pools with different regression slopes (Fig. 7).

413

4 Discussion

415   4.1 Assumptions of the C cycle models and validity of this analysis

416   This analysis is built upon eq. 1, which represents the majority of terrestrial C cycle

417   models developed in the past decades (Manzoni and Porporato, 2009; Sierra and Müller, 2015).

418   Those models have several assumptions, which may influence the validity of this analysis. First,

419   those models assume that donor pools control C transfers among pools and decomposition

420   follows 1st-order decay functions (Assumption 1). This assumption is built upon observations

421   from litter and SOC decomposition. Analysis of data from nearly 300 studies of litter

422   decomposition (Zhang et al., 2008), about 500 studies of soil incubation (Schädel et al., 2014;

423   Xu et al., 2016), more than 100 studies of forest succession (Yang et al., 2011), and restoration

424   (Matamala et al., 2008) almost all suggests that the 1st-order decay function captures

425   macroscopic patterns of land C dynamics. Even so, its biological, chemical and physical

426   underpinnings need more study (Luo et al., 2016). This assumption has recently been challenged

427   by a notion that microbes are actively involved in decomposition processes. To describe the

428   active roles of microbes in organic C decomposition, a suite of nonlinear microbial models has

429   been proposed using Michaelis-Menten or reverse Michaelis-Menten equations (Allison et al.,

430   2010; Wieder et al., 2013). Those nonlinear models exhibit unique behaviors of modeled

431   systems, such as damped oscillatory responses of soil C dynamics to small perturbations and

432   insensitivity of the equilibrium pool sizes of litter or soil carbon to inputs (Li et al., 2014; Wang

433   et al., 2014; 2016). Oscillations have been documented for single enzymes at timescales between

434   10^{-4} to 10 seconds (English et al., 2006; Goldbeter, 2013; Xie, 2013). Over longer timescales

435   with mixtures of large diversity of enzyme-substrate complexes in soil, oscillations may be likely

436   averaged out so that the 1st order decay functions may well approximate these average dynamics

437   of organic matter decomposition (Sierra and Müller, 2015).

438   Second, those models all assume that multiple pools can adequately approximate

439   transformation, decomposition, and stabilization of SOC in the real world (Assumption 2). The

440   classic SOC model, CENTURY, uses three conceptual pools, active, slow, and passive SOC, to

441   represent SOC dynamics (Parton et al., 1987). Several models define pools that are

442   corresponding to measurable SOC fractions to match experimental observation with modeling

443   analysis (Smith et al., 2002; Stewart et al., 2008). Carbon transformation in soil over time has

444   also been described by a partial differential function of SOM quality (Bosatta and Ågren, 1991;

445   Ågren and Bosatta, 1996). The latter quality model describes the external inputs of C with

446   certain quality, C loss due to decomposition, and the internal transformations of the quality of

447   soil organic matter. It has been shown that multi-pool models can approximate the partial

448   differential function or continuous quality model as the number of pools increases (Bolker et al.,

449   1998; Sierra and Müller, 2015).

450   Assumption 3 is on partitioning coefficients of C input (i.e., elements in vector B) and C

451   transformation among plant, litter, and soil pools (i.e., elements in the matrix, $A\xi(t)K$). Some of

452   the terrestrial C cycle models assume that elements in vector B, and matrices A and K are

453   constants. All the factors or processes that vary with time are represented in the diagonal matrix

454   $\xi(t)$. In the real world, C transformation are influenced by environmental variables (e.g.,

455   temperature, moisture, oxygen, N, phosphorus, and acidity varying with soil profile, space, and

456   time), litter quality (e.g., lignin, cellulose, N, or their relative content), organomineral properties

457   of SOC (e.g., complex chemical compounds, aggregation, physiochemical binding and

458   protection, reactions with inorganic, reactive surfaces, and sorption), and microbial attributes

459   (e.g., community structure, functionality, priming, acclimation, and other physiological

460   adjustments) (Luo et al., 2016). It is not practical to incorporate all of those factors and processes

461   into one model. Only a subset of them is explicitly expressed while the majority is implicitly

462   embedded in the C cycle models. Empirical studies have suggested that temperature, moisture,

463   litter quality, and soil texture are primary factors that control C transformation processes of

464   decomposition and stabilization (Burke et al., 1989; Adair et al., 2008; Zhang et al., 2008; Xu et

465   al., 2012; Wang et al., 2013). Nitrogen influences C cycle processes mainly through changes in

466   photosynthetic C input, C partitioning, and decomposition. It is yet to identify how other major

467   factors and processes, such as microbial activities and organomineral protection, regulate C

468   transformation.

469   Assumption 4 is that terrestrial C cycle models use different response functions (i.e.,

470   different $\xi(t)$ in eq. 1) to represent C cycle responses to external variables. As temperature

471   modifies almost all processes in the C cycle, different formulations, including exponential,

472   Arrhenius, and optimal response functions, have been used to describe C cycle responses to

473   temperature changes in different models (Lloyd and Taylor, 1994; Jones et al., 2005; Sierra and

474   Müller, 2015). Different response functions are used to connect C cycle processes with moisture,

475   nutrient availability, soil clay content, litter quality, and other factors. Different formulations of

476   response functions may result in substantially different model projections (Exbrayat et al., 2013)

477   but unlikely change basic dynamics of the model behaviors.

478   Assumption 5 is that disturbance events are represented in models in different ways

479   (Grosse et al., 2011; West et al., 2011; Goetz et al., 2012; Hicke et al., 2012). Fire, extreme

480   drought, insect outbreaks, land management, and land cover and land use change influence

481   terrestrial C dynamics via 1) altering rate processes, for example, gross primary productivity

482   (GPP), growth, tree mortality, or heterotrophic respiration; 2) modifying microclimatic

483   environments; 3) transferring C from one pool to another (e.g., from live to dead pools during

484   storms or release to the atmosphere with fire) (Kloster et al., 2010; Thonicke et al., 2010; Luo

485   and Weng, 2011; Prentice et al., 2011; Weng et al., 2012). Those disturbance influences can be

486   represented in terrestrial C cycle models through changes in parameter values, environmental

487   scalars, and/or discrete C transfers among pools of eq. 1 (Luo and Weng 2011). While eq. 1 does

488   not explicitly incorporate disturbances for their influences on land C cycle, Weng et al. (2012)

489   developed a disturbance regime model that combines eq. 1 with frequency distributions of

490   disturbance severity and intervals to quantify net biome exchanges.

491   The sixth assumption that those models make is that the lateral C fluxes through erosion

492 or local C drainage is negligible so that eq (1) can approximate terrestrial C cycle over space. If

493 soil erosion is substantial enough to be modeled with horizontal movement of C, a third

494 dimension should be added in addition to two-dimensional transfers in classic models.

495   Our analysis on transient dynamics of terrestrial C cycle is valid unless some of the

496 assumptions are violated. Assumption 1 on the 1st-order decay function of decomposition

497 appears to be supported by thousands of datasets. It is a burden on microbiologists to identify

498 empirical evidence to support the nonlinear microbial models. Assumption 2 may not affect the

499 validity of our analysis no matter how C pools are divided in the ecosystems. Our analysis in this

500 study is applicable no matter whether elements are time-varying or constant in vector B and

501 matrices A and K as in assumption 3. Neither assumption 4 nor 5 would affect the analysis in this

502 study. The environmental scalar, $\xi(t)$, as related to assumption 4 can be any forms in the derived

503 equations (e.g., eq. 2). Disturbances of fire, land use, and extreme drought change rate processes

504 but do not alter the basic formulation of eq. 1. If soil erosion and lateral transportation of C

505 become a major research objective, Eq. (1) can no longer be analyzed to understand the

506 mathematical foundation underlying transient dynamics of terrestrial C cycle.

507

508 **4.2 Carbon storage capacity**

509   One of the two components this analysis introduces to understand transient dynamics of

510 terrestrial C storage is the C storage capacity (Eq. 2). Olson (1963) is probably among the first

511 who systematically analyzed C storage dynamics at forest floor as functions of litter production

512 and decomposition. He collected data of annual litter production and approximately steady-state

513 organic C storage at forest floor, from which decomposition rates were estimated for a variety of

514 ecosystems from Ghana in the tropics to alpine forests in California. Using the relationships

515   among litter production, decomposition, and C storage, Olson (1963) explored several issues,

516   such as decay without input, accumulation with continuous or discrete annual litter fall, and

517   adjustments in production and decay parameters during forest succession. His analysis

518   approximated the steady-state C storage as the C input times the inverse of decomposition (i.e.,

519   residence time). The steady-state C storage is also considered the maximal amount of C that a

520   forest can store.

521   This study is not only built upon Olson's analysis but also expands it at least in two

522   aspects. First, we similarly define the C storage capacity (i.e., eqs. 5a and 5b). Those equations

523   can be applied to a whole ecosystem with multiple C pools while Olson's analysis is for one C

524   pool. Second, Olson (1963) treated the C input and decomposition rate as yearly constants at a

525   given location even though they varied with locations. This study considers both C input and rate

526   of decomposition being time dependent. A dynamical system with its input and parameters being

527   time dependent mathematically becomes a nonautonomous system (Kloeden and Rasmussen,

528   2011). As terrestrial C cycle under global change is transient, we need to treat it a

529   nonautonomous system to better understand the properties of transient dynamics. Olson (1963)

530   approximated the non-autonomous system at the yearly time scale without global change so as to

531   effectively understand properties of the steady-state C storage at the forest floor. In comparison,

532   eqs. 5a and b are not only more general but also essential for understanding transient dynamics

533   of the terrestrial C cycle in response to global change.

534   Under the transient dynamics, the C storage capacity as defined by eqs 5a and b still sets

535   the maximal amount of C that one ecosystem can store at time t. This capacity represents

536   instantaneous responses of ecosystem C cycle to external forcing via changes in both C input and

537   residence time, and thus varies within one day, over seasons of a year, and interannually over

538   longer time scales as forcings vary. The variation of the C storage capacity can result from cyclic

539   environmental changes (e.g., dial and seasonal changes), directional global change (e.g., rising

540   atmospheric CO_2, nitrogen deposition, altered precipitation, and warming), disturbance events,

541   disturbance regime shifts, and changing vegetation dynamics (Luo and Weng, 2011). As the

542   capacity sets the maximal amount of C storage (Fig. 2a), it is a moving attractor toward which

543   the current C storage chases. When the capacity is larger than the C storage itself, C storage

544   increases. Otherwise, the C storage decreases.

545

546   **4.3 Carbon storage potential**

547   The C storage potential represents the internal capability to equilibrate the current C storage with

548   the capacity. Bogeochemically, the C storage potential represents re-distribution of net C pool

549   change, $X'(t)$, of individual pools through a network of pools with different residence times as

550   connected by C transfers from one pool to the others through all the pathways. The potential is

551   conceptually equivalent to the magnitude of disequilibrium as discussed by Luo and Weng

552   (2011).

553   Extensive studies have been done to quantify terrestrial C sequestration. The most

554   commonly estimated quantities for C sequestration include net ecosystem exchange (NEE), C

555   stocks in ecosystems (i.e., plant biomass and SOC) and their changes (Baldocchi et al., 2001; Pan

556   et al., 2013). This study, for the first time, offers the theoretical basis to estimate the terrestrial C

557   storage potential in at least two approaches: (1) the product of chasing time and net C pool

558   change with eqs. 6a and 6b; and (2) the difference between the C storage capacity and the C

559   storage itself with eqs. 6c. Since the time-varying C storage capacity is fully defined by

560   residence time and C input at any given time, C storage potential can be estimated from three

561   quantities: C input, residence time, and C storage.

562   To effectively quantify the C storage potential in terrestrial ecosystems, we need various

563   data sets from experimental and observatory studies to be first assimilated into models. For

564   example, data from Harvard Forest were first used to constrain the TECO model. The

565   constrained model was used to explore changes in ecosystem C storage in response to global

566   change scenario, RCP8.5. That scenario primarily stimulated NPP, which increased from 1.06 to

567   1.8 kg C m^{-2} yr^{-1} in the Harvard Forest (Fig. 5b). Although climate warming decreased

568   ecosystem C residence time in the Harvard Forest, the substantial increases in NPP resulted in

569   increases in the C storage potential over time.

570

571   **4.4 Novel approaches to model evaluation and improvement**

572   Our analysis of transient C cycle dynamics offers new approaches to understand,

573   evaluate, diagnose, and improve land C cycle models. We have demonstrated that many global

574   land C cycle models can be exactly represented by the matrix equation (Eqs. 1 and 2) (i.e.,

575   physical emulators). As a consequence, outputs of all those models can be placed into a three

576   dimensional (3D) space (Eq. 7) to measure their differences. In addition, components of land C

577   cycle models are simulated in a mutually independent fashion so that modeled C storage can be

578   decomposed into traceable components for traceability analysis. Moreover, the physical

579   emulators computationally enable data assimilation to constrain complex models.

580   *Physical Emulators of land C cycle models* We have developed matrix representations

581   (i.e., physical emulators) of CABLE, LPJ-GUESS, CLM3.5, CLM 4.0, CLM4.5, BEPS, and

582   TECO (Xia et al., 2013; Hararuk et al., 2014; Ahlström et al., 2015; Chen et al., 2015). The

583   emulators can exactly replicate simulations of C pools and fluxes with their original models

584 when driven by a limited set of inputs from the full model (GPP, soil temperature, and soil

585 moisture) (Fig. 1b and 1c). However, the physical emulators differ for different models as the

586 elements of each matrix could be differently parameterized or formulized in different models.

587 Also, different models usually have different pool-flux structures, leading to different non-zero

588 elements in the *A* matrix. Nonetheless, the physical emulators make complex models analytically

589 clear and, therefore, give us a way to understand the effects of forcing, model structures, and

590 parameters on modeled ecosystem processes. They greatly simplify the task of understanding the

591 dynamics of submodels and interactions between them. The emulators allow us to analyze model

592 results in the 3D parameter space and the traceability framework.

593   *Parameter space of C cycle dynamics* Eq. 7 indicates that transient dynamics of modeled

594 C storage are determined by three parameters: C input, residence time, and C storage potential.

595 The 3D parameter space offers one novel approach to uncertainty analysis of global C cycle

596 models. As global land models incorporate more and more processes to simulate C cycle

597 responses to global change, it becomes very difficult to understand or evaluate complex model

598 behaviors. As such, differences in model projections cannot be easily diagnosed and attributed to

599 their sources (Chatfield, 1995; Friedlingstein et al., 2006; Luo et al., 2009). Eq. 7 can help

600 diagnose and evaluate complex models by placing all modeling results within one common

601 parameter space in spite of the fact that individual global models may have tens or hundreds of

602 parameters to represent C cycle processes as affected by many abiotic and biotic factors (Luo et

603 al., 2016). The 3D space can be used to measure how and how much the models diverge.

604   *Traceability analysis* The two terms on the right side of eq. 2 can be decomposed into

605 traceable components (Xia et al., 2013) so as to identify sources of uncertainty in C cycle model

606 projections. Model intercomparison projects (MIPs) all illustrate great spreads in projected land

607   C sink dynamics across models (Todd-Brown et al., 2013; Tian et al., 2015). It has been

608   extremely challenging to attribute the uncertainty to sources. Placing simulation results of a

609   variety of C cycle models within one common parameter space can measure how much the

610   model differences are in a common metrics (Eq. 7). The measured differences can be further

611   attributed to sources in model structure, parameter, and forcing fields with traceability analysis

612   (Xia et al., 2013; Rafique et al., 2014; Ahlström et al., 2015; Chen et al., 2015). The traceability

613   analysis also can be used to evaluate effectiveness of newly incorporated modules into existing

614   models, such as adding the N module on simulated C dynamics (Xia et al., 2013) and locate the

615   origin of model ensemble uncertainties to external forcing vs. model structures and parameters

616   (Ahlström et al., 2015).

617   *Constrained estimates of terrestrial C sequestration* Traditionally, global land C sink is

618   indirectly estimated from airborne fraction of C emission and ocean uptake. Although many

619   global land models have been developed to estimate land C sequestration, a variety of MIPs

620   indicate that model predictions widely vary among them and do not fit observations well

621   (Schwalm et al., 2010; Luo et al., 2015; Tian et al., 2015). Moreover, the prevailing practices in

622   the modeling community, unfortunately, may not lead to significant enhancements in our

623   confidence on model predictions. For example, incorporating an increasing number of processes

624   that influence the C cycle may represent the real-world phenomena more realistically but makes

625   the models more complex and less tractable. MIPs have effectively revealed the extent of the

626   differences between model predictions (Schwalm et al., 2010; Keenan et al., 2012; De Kauwe et

627   al., 2013) but provide limited insights into sources of model differences (but see Medlyn et al.

628   2015). The physical emulators make data assimilation computationally feasible for global C

629   cycle models (Hararuk *et al.* 2014; 2015) and thus offer the possibility to generate independent

630   yet constrained estimates of global land C sequestration to be compared with the indirect

631   estimate from the airborne fraction of C emission and ocean uptake. With the emulators, we can

632   assimilate most of the C flux- and pool-related datasets into those models to better constrain

633   global land C sink dynamics.

634

635   **5 Concluding remarks**

636   In this study we theoretically explored the transient dynamics of terrestrial C storage. Our

637   analysis indicates that transient C storage dynamics can be partitioned into two components: the

638   C storage capacity and the C storage potential. The capacity, which is the product of C input and

639   residence time, represents their instantaneous responses to a state of external forcing at a given

640   time. Thus, the C storage capacity quantifies the maximum amount of C that an ecosystem can

641   store at the given environmental condition at a point of time. Thus it varies diurnally, seasonally,

642   and interannually as environmental condition changes.

643   The C storage potential is the difference between the capacity and the current C storage

644   and thus measures the magnitude of disequilibrium in the terrestrial C cycle (Luo and Weng,

645   2011). The storage potential represents the internal capability (or recovery force) of the

646   terrestrial C cycle to influence the change in C storage in the next time step through

647   redistribution of net C pool changes in a network of multiple pools with different residence

648   times. The redistribution drives the current C storage towards the capacity and thus equilibrates

649   C efflux with influx.

650   The two components of land C storage dynamics represent interactions of external forces

651   (via changes in the capacity) and internal capability of the land C cycle (via changes in the C

652   storage potential) to generate complex phenomena of C cycle dynamics, such as fluctuations,

653   directional changes, and tipping points, in the terrestrial ecosystems. From a system perspective,

654   these complex phenomena could not be generated by relatively simple internal processes but are

655   mostly caused by multiple environmental forcing variables interacting with internal processes

656   over different temporal and spatial scales as explained by Luo and Weng (2011) and Luo et al.

657   (2015). Note that while those internal processes can be mathematically represented with a

658   relatively simple formula, their ecological and biological underpinnings can be very complex.

659   The theoretical framework developed in this study has the potential to revolutionize

660   model evaluation. Our analysis indicates that the matrix equation as in eq. 1 or 2 can adequately

661   emulate most of the land C cycle models. Indeed, we have developed physical emulators of

662   several global land C cycle models. In addition, predictions of C dynamics with complex land

663   models can be placed in a 3D parameter space as a common metric to measure how much model

664   predictions are different. The latter can be traced to its source components by decomposing

665   model predictions to a hierarchy of traceable components. Moreover, the physical emulators

666   make it computationally possible to assimilate multiple sources of data to constrain predictions

667   of complex models.

668   The theoretical framework we developed in this study can well explain dynamics of C

669   storage in response to cyclic seasonal change in external forcings (e.g., Figs. 2 and 3), climate

670   change, and rising atmospheric CO_2 (Fig. 5). It can also explain responses of ecosystem C

671   storage to disturbances and other global change factors, such as nitrogen deposition, land use

672   changes, and altered precipitation. The theoretical framework is simple and straightforward but

673   able to characterize the direction and rate of C storage change, which are arguably among the

674   most critical issues for quantifying terrestrial C sequestration. Future research should explicitly

675   incorporate stochastic disturbance regime shifts (e.g., Weng et al., 2012) and vegetation

676 dynamics (Moorcroft et al., 2001; Purves and Pacala, 2008; Fisher et al., 2010; Weng et al.,

677 2015) into this theoretical framework to explore their theoretical issues related to

678 biogeochemistry.

679

680 **6 Code availability**

681 Computer code of the TECO model and its physical emulator are available at

682 http://ecolab.ou.edu/download/TECO%20Emulator.php

683

684

693

694 **References**

695 Adair, E. C., Parton, W. J., Del Grosso, S. J., Silver, W. L., Harmon, M. E., Hall, S. A., Burke, I.
696 C., and Hart, S. C.: Simple three-pool model accurately describes patterns of long-term litter
697 decomposition in diverse climates, Global Change Biol, 14, 2636-2660, 2008.

698 Ågren, G. I. and Bosatta, E.: Quality: A bridge between theory and experiment in soil organic
699 matter studies, Oikos, 76, 522-528, 1996.

700 Ahlström, A., Xia, J. Y., Arneth, A., Luo, Y. Q., and smith, B.: Importance of vegetation
701 dynamics for future terrestrial carbon cycling, Environmental Research Letters, 10, 054019
702 doi:054010.051088/051748-059326/054010/054015/054019, 2015.

703 Allison, S. D., Wallenstein, M. D., and Bradford, M. A.: Soil-carbon response to warming
704 dependent on microbial physiology, Nat Geosci, 3, 336-340, 2010.

705 Baldocchi, D., Falge, E., Gu, L. H., Olson, R., Hollinger, D., Running, S., Anthoni, P.,
706 Bernhofer, C., Davis, K., Evans, R., Fuentes, J., Goldstein, A., Katul, G., Law, B., Lee, X. H.,
707 Malhi, Y., Meyers, T., Munger, W., Oechel, W., U, K. T. P., Pilegaard, K., Schmid, H. P.,
708 Valentini, R., Verma, S., Vesala, T., Wilson, K., and Wofsy, S.: FLUXNET: A new tool to study
709 the temporal and spatial variability of ecosystem-scale carbon dioxide, water vapor, and energy
710 flux densities, B Am Meteorol Soc, 82, 2415-2434, 2001.

711 Bolker, B. M., Pacala, S. W., and Parton, W. J.: Linear analysis of soil decomposition: Insights
712 from the century model, Ecol Appl, 8, 425-439, 1998.

713 Borer, E. T., Harpole, W. S., Adler, P. B., Lind, E. M., Orrock, J. L., Seabloom, E. W., and
714 Smith, M. D.: Finding generality in ecology: a model for globally distributed experiments,
715 Methods in Ecology and Evolution, 5, 65-73, 2014.

716 Bosatta, E. and Ågren, G. I.: Dynamics of carbon and nitrogen in the organic matter of the soil: a
717 generic theory, American Naturalist, 1991. 227-245, 1991.

718 Burke, I. C., Yonker, C. M., Parton, W. J., Cole, C. V., Flach, K., and Schimel, D. S.: Texture,
719 Climate, and Cultivation Effects on Soil Organic-Matter Content in Us Grassland Soils, Soil Sci
720 Soc Am J, 53, 800-805, 1989.

721 Canadell, J. G., Le Quéré, C., Raupach, M. R., Field, C. B., Buitenhuis, E. T., Ciais, P., Conway,
722 T. J., Gillett, N. P., Houghton, R. A., and Marland, G.: Contributions to accelerating atmospheric
723 CO2 growth from economic activity, carbon intensity, and efficiency of natural sinks,
724 Proceedings of the National Academy of Sciences, 104, 18866-18870, 2007.

725 Caswell, H.: Prospective and retrospective perturbation analyses: their roles in conservation
726 biology, Ecology, 81, 619-627, 2000.

727 Chatfield, C.: Model uncertainty, data mining and statistical-inference, Journal of the Royal
728 Statistical Society Series a-Statistics in Society, 158, 419-466, 1995.

729 Chen, Y., Xia, J., Sun, Z., Li, J., Luo, Y., Gang, C., and Wang, Z.: The role of residence time in
730 diagnostic models of global carbon storage capacity: model decomposition based on a traceable
731 scheme, Scientific reports, 5, 2015.

732 Ciais, P., Gasser, T., Paris, J. D., Caldeira, K., Raupach, M. R., Canadell, J. G., Patwardhan, A.,
733 Friedlingstein, P., Piao, S. L., and Gitz, V.: Attributing the increase in atmospheric CO_2 to
734 emitters and absorbers, Nat Clim Change, 3, 926-930, 2013.

De Kauwe, M. G., Medlyn, B. E., Zaehle, S., Walker, A. P., Dietze, M. C., Hickler, T., Jain, A. K., Luo, Y., Parton, W. J., Prentice, I. C., Smith, B., Thornton, P. E., Wang, S., Wang, Y.-P., Wårlind, D., Weng, E., Crous, K. Y., Ellsworth, D. S., Hanson, P. J., Seok Kim, H., Warren, J. M., Oren, R., and Norby, R. J.: Forest water use and water use efficiency at elevated CO_2: a model-data intercomparison at two contrasting temperate forest FACE sites, Global Change Biology, 19, 1759-1779, 2013.

English, B. P., Min, W., Van Oijen, A. M., Lee, K. T., Luo, G., Sun, H., Cherayil, B. J., Kou, S., and Xie, X. S.: Ever-fluctuating single enzyme molecules: Michaelis-Menten equation revisited, Nature chemical biology, 2, 87-94, 2006.

Exbrayat, J. F., Pitman, A. J., Zhang, Q., Abramowitz, G., and Wang, Y. P.: Examining soil carbon uncertainty in a global model: response of microbial decomposition to temperature, moisture and nutrient limitation, Biogeosciences, 10, 7095-7108, 2013.

Farquhar, G., von Caemmerer, S. v., and Berry, J.: A biochemical model of photosynthetic CO_2 assimilation in leaves of C3 species, Planta, 149, 78-90, 1980.

Fisher, R., McDowell, N., Purves, D., Moorcroft, P., Sitch, S., Cox, P., Huntingford, C., Meir, P., and Ian Woodward, F.: Assessing uncertainties in a second‐generation dynamic vegetation model caused by ecological scale limitations, New Phytol, 187, 666-681, 2010.

Fraser, L. H., Henry, H. A., Carlyle, C. N., White, S. R., Beierkuhnlein, C., Cahill, J. F., Casper, B. B., Cleland, E., Collins, S. L., and Dukes, J. S.: Coordinated distributed experiments: an emerging tool for testing global hypotheses in ecology and environmental science, Frontiers in Ecology and the Environment, 11, 147-155, 2013.

Friedlingstein, P., Cox, P., Betts, R., Bopp, L., Von Bloh, W., Brovkin, V., Cadule, P., Doney, S., Eby, M., Fung, I., Bala, G., John, J., Jones, C., Joos, F., Kato, T., Kawamiya, M., Knorr, W., Lindsay, K., Matthews, H. D., Raddatz, T., Rayner, P., Reick, C., Roeckner, E., Schnitzler, K. G., Schnur, R., Strassmann, K., Weaver, A. J., Yoshikawa, C., and Zeng, N.: Climate-carbon cycle feedback analysis: Results from the (CMIP)-M-4 model intercomparison, J Climate, 19, 3337-3353, 2006.

Goetz, S. J., Bond-Lamberty, B., Law, B. E., Hicke, J. A., Huang, C., Houghton, R. A., McNulty, S., O'Halloran, T., Harmon, M., Meddens, A. J. H., Pfeifer, E. M., Mildrexler, D., and Kasischke, E. S.: Observations and assessment of forest carbon dynamics following disturbance in North America, J Geophys Res-Biogeo, 117, 2012.

Goldbeter, A.: Oscillatory enzyme reactions and Michaelis–Menten kinetics, FEBS letters, 587, 2778-2784, 2013.

Grosse, G., Harden, J., Turetsky, M., McGuire, A. D., Camill, P., Tarnocai, C., Frolking, S., Schuur, E. A. G., Jorgenson, T., Marchenko, S., Romanovsky, V., Wickland, K. P., French, N., Waldrop, M., Bourgeau-Chavez, L., and Striegl, R. G.: Vulnerability of high-latitude soil organic carbon in North America to disturbance, J Geophys Res-Biogeo, 116, 2011.

Hammerling, D. M., Michalak, A. M., and Kawa, S. R.: Mapping of CO_2 at high spatiotemporal resolution using satellite observations: Global distributions from OCO-2, J Geophys Res-Atmos, 117, do6306, 2012.

Hararuk, O., Smith, M. J., and Luo, Y. Q.: Microbial models with data-driven parameters predict stronger soil carbon responses to climate change, Global Change Biology, 21, 2439-2453, 2015.

Hararuk, O., Xia, J. Y., and Luo, Y. Q.: Evaluation and improvement of a global land model against soil carbon data using a Bayesian Markov chain Monte Carlo method, J Geophys Res-Biogeo, 119, 403-417, 2014.

Harley, P., Thomas, R., Reynolds, J., and Strain, B.: Modelling photosynthesis of cotton grown in elevated CO_2, Plant, Cell & Environment, 15, 271-282, 1992.

Hicke, J. A., Allen, C. D., Desai, A. R., Dietze, M. C., Hall, R. J., Hogg, E. H., Kashian, D. M., Moore, D., Raffa, K. F., Sturrock, R. N., and Vogelmann, J.: Effects of biotic disturbances on forest carbon cycling in the United States and Canada, Global Change Biol, 18, 7-34, 2012.

Jenkinson, D., Hart, P., Rayner, J., and Parry, L.: Modelling the turnover of organic matter in long-term experiments at Rothamsted, 1987. 1987.

Jones, C., McConnell, C., Coleman, K., Cox, P., Falloon, P., Jenkinson, D., and Powlson, D.: Global climate change and soil carbon stocks; predictions from two contrasting models for the turnover of organic carbon in soil, Global Change Biol, 11, 154-166, 2005.

Keenan, T. F., Baker, I., Barr, A., Ciais, P., Davis, K., Dietze, M., Dragoni, D., Gough, C. M., Grant, R., Hollinger, D., Hufkens, K., Poulter, B., McCaughey, H., Raczka, B., Ryu, Y., Schaefer, K., Tian, H., Verbeeck, H., Zhao, M., and Richardson, A. D.: Terrestrial biosphere model performance for inter-annual variability of land-atmosphere CO_2 exchange, Global Change Biol, 18, 1971-1987, 2012.

Kloeden, P. E. and Rasmussen, M.: Nonautonomous dynamical systems, American Mathematical Society, 2011.

Kloster, S., Mahowald, N. M., Randerson, J. T., Thornton, P. E., Hoffman, F. M., Levis, S., Lawrence, P. J., Feddema, J. J., Oleson, K. W., and Lawrence, D. M.: Fire dynamics during the 20th century simulated by the Community Land Model, Biogeosciences, 7, 2010.

Le Quéré, C., Moriarty, R., Andrew, R. M., Canadell, J. G., Sitch, S., Korsbakken, J. I., Friedlingstein, P., Peters, G. P., Andres, R. J., Boden, T. A., Houghton, R. A., House, J. I., Keeling, R. F., Tans, P., Arneth, A., Bakker, D. C. E., Barbero, L., Bopp, L., Chang, J., Chevallier, F., Chini, L. P., Ciais, P., Fader, M., Feely, R. A., Gkritzalis, T., Harris, I., Hauck, J., Ilyina, T., Jain, A. K., Kato, E., Kitidis, V., Klein Goldewijk, K., Koven, C., Landschützer, P., Lauvset, S. K., Lefèvre, N., Lenton, A., Lima, I. D., Metzl, N., Millero, F., Munro, D. R., Murata, A., Nabel, J. E. M. S., Nakaoka, S., Nojiri, Y., O'Brien, K., Olsen, A., Ono, T., Pérez, F. F., Pfeil, B., Pierrot, D., Poulter, B., Rehder, G., Rödenbeck, C., Saito, S., Schuster, U., Schwinger, J., Séférian, R., Steinhoff, T., Stocker, B. D., Sutton, A. J., Takahashi, T., Tilbrook, B., van der Laan-Luijkx, I. T., van der Werf, G. R., van Heuven, S., Vandemark, D., Viovy, N.,

810   Wiltshire, A., Zaehle, S., and Zeng, N.: Global Carbon Budget 2015, Earth Syst. Sci. Data, 7,
811   349-396, 2015.

812   Li, J. W., Luo, Y. Q., Natali, S., Schuur, E. A. G., Xia, J. Y., Kowalczyk, E., and Wang, Y. P.:
813   Modeling permafrost thaw and ecosystem carbon cycle under annual and seasonal warming at an
814   Arctic tundra site in Alaska, J Geophys Res-Biogeo, 119, 1129-1146, 2014.

815   Lloyd, J. and Taylor, J. A.: On the Temperature-Dependence of Soil Respiration, Funct Ecol, 8,
816   315-323, 1994.

817   Luo, Y., Ahlström, A., Allison, S. D., Batjes, N. H., Brovkin, V., Carvalhais, N., Chappell, A.,
818   Ciais, P., Davidson, E. A., Finzi, A., Georgiou, K., Guenet, B., Hararuk, O., Harden, J. W., He,
819   Y., Hopkins, F., Jiang, L., Koven, C., Jackson, R. B., Jones, C. D., Lara, M. J., Liang, J.,
820   McGuire, A. D., Parton, W., Peng, C., Randerson, J. T., Salazar, A., Sierra, C. A., Smith, M. J.,
821   Tian, H., Todd-Brown, K. E. O., Torn, M., van Groenigen, K. J., Wang, Y. P., West, T. O., Wei,
822   Y., Wieder, W. R., Xia, J., Xu, X., Xu, X., and Zhou, T.: Toward more realistic projections of
823   soil carbon dynamics by Earth system models, Global Biogeochemical Cycles, 30, 40-56, 2016.

824   Luo, Y., Weng, E., Wu, X., Gao, C., Zhou, X., and Zhang, L.: Parameter identifiability,
825   constraint, and equifinality in data assimilation with ecosystem models, Ecological Applications,
826   19, 571-574, 2009.

827   Luo, Y. and Zhou, X.: Soil respiration and the environment, Academic Press, Burlington, MA,
828   USA, 2006.

829   Luo, Y. Q., Keenan, T. F., and Smith, M.: Predictability of the terrestrial carbon cycle, Global
830   Change Biol, 21, 1737-1751, 2015.

831   Luo, Y. Q., Ogle, K., Tucker, C., Fei, S. F., Gao, C., LaDeau, S., Clark, J. S., and Schimel, D. S.:
832   Ecological forecasting and data assimilation in a data-rich era, Ecol Appl, 21, 1429-1442, 2011.

833   Luo, Y. Q. and Weng, E. S.: Dynamic disequilibrium of the terrestrial carbon cycle under global
834   change, Trends Ecol Evol, 26, 96-104, 2011.

835   Luo, Y. Q., White, L. W., Canadell, J. G., DeLucia, E. H., Ellsworth, D. S., Finzi, A. C., Lichter,
836   J., and Schlesinger, W. H.: Sustainability of terrestrial carbon sequestration: A case study in
837   Duke Forest with inversion approach, Global Biogeochem Cy, 17, 2003.

838   Luo, Y.Q., Wu, L., Andrews, J.A., White, L., Matamala, R., Schafer, K.V.R., and Schlesinger,
839   W. H. Elevated CO2 differentiates ecosystem carbon processes: Deconvolution analysis of Duke
840   Forest FACE data.. Ecological Monographs. **71**:357-376, 2001.

841   Manzoni, S. and Porporato, A.: Soil carbon and nitrogen mineralization: theory and models
842   across scales, Soil Biology and Biochemistry, 41, 1355-1379, 2009.

843   Matamala, R., Jastrow, J. D., Miller, R. M., and Garten, C. T.: Temporal changes in C and N
844   stocks of restored prairie: Implications for C sequestration strategies, Ecological Applications,
845   18, 1470-1488, 2008.

846 Medlyn, B. E., Zaehle, S., De Kauwe, M. G., Walker, A. P., Dietze, M. C., Hanson, P. J.,
847 Hickler, T., Jain, A. K., Luo, Y., Parton, W., Prentice, I. C., Thornton, P. E., Wang, S., Wang,
848 Y.-P., Weng, E., Iversen, C. M., McCarthy, H. R., Warren, J. M., Oren, R., and Norby, R. J.:
849 Using ecosystem experiments to improve vegetation models, Nature Climate Change, 5, 528-
850 534, 2015.

851 Moorcroft, P., Hurtt, G., and Pacala, S. W.: A method for scaling vegetation dynamics: the
852 ecosystem demography model (ED), Ecol Monogr, 71, 557-586, 2001.

853 Oleson, K., Lawrence, D., Bonan, G., Drewniak, B., Huang, M., Koven, C., Levis, S., Li, F.,
854 Riley, W., and Subin, Z.: Technical description of version 4.5 of the Community Land Model
855 (CLM), National Center for Atmospheric Research, Boulder, Colorado, 2013.

856 Olson, J. S.: Energy storage and the balance of producers and decomposers in ecological
857 systems, Ecology, 44, 322-331, 1963.

858 Pan, Y., Birdsey, R. A., Phillips, O. L., and Jackson, R. B.: The structure, distribution, and
859 biomass of the world's forests, Annual Review of Ecology, Evolution, and Systematics, 44, 593-
860 622, 2013.

861 Parolari A., Porporato A., Forest soil carbon and nitrogen cycles under biomass harvest: stability,
862 transient response, and feedback. *Ecological Modelling*, 329, 64-76, 2016
863

864 Parton, W. J., Schimel, D. S., Cole, C. V., and Ojima, D. S.: Analysis of Factors Controlling Soil
865 Organic-Matter Levels in Great-Plains Grasslands, Soil Sci Soc Am J, 51, 1173-1179, 1987.

866 Parton, W. J., Scurlock, J. M. O., Ojima, D. S., Gilmanov, T. G., Scholes, R. J., Schimel, D. S.,
867 Kirchner, T., Menaut, J. C., Seastedt, T., Moya, E. G., Kamnalrut, A., and Kinyamario, J. I.:
868 Observations and Modeling of Biomass and Soil Organic-Matter Dynamics for the Grassland
869 Biome Worldwide, Global Biogeochem Cy, 7, 785-809, 1993.

870 Parton, W. J., Stewart, J. W. B., and Cole, C. V.: Dynamics of C, N, P and S in Grassland Soils -
871 a Model, Biogeochemistry, 5, 109-131, 1988.

872 Potter, C. S., Randerson, J. T., Field, C. B., Matson, P. A., Vitousek, P. M., Mooney, H. A., and
873 Klooster, S. A.: Terrestrial Ecosystem Production: a Process Model-Based on Global Satellite
874 and Surface Data, Global Biogeochem Cy, 7, 811-841, 1993.

875 Prentice, I. C., Kelley, D. I., Foster, P. N., Friedlingstein, P., Harrison, S. P., and Bartlein, P. J.:
876 Modeling fire and the terrestrial carbon balance, Global Biogeochem Cy, 25, 2011.

877 Purves, D. and Pacala, S.: Predictive models of forest dynamics, Science, 320, 1452-1453, 2008.

878 Rafique, R., Xia, J., Hararuk, O., and Luo, Y.: Structural analysis of three global land models on
879 carbon cycle simulations using a traceability framework, Biogeosciences Discussions, 11, 9979-
880 10014, 2014.

Rustad, L., Campbell, J., Marion, G., Norby, R., Mitchell, M., Hartley, A., Cornelissen, J., and Gurevitch, J.: A meta-analysis of the response of soil respiration, net nitrogen mineralization, and aboveground plant growth to experimental ecosystem warming, Oecologia, 126, 543-562, 2001.

Schwalm, C. R., Williams, C. A., Schaefer, K., Anderson, R., Arain, M. A., Baker, I., Barr, A., Black, T. A., Chen, G., Chen, J. M., Ciais, P., Davis, K. J., Desai, A., Dietze, M., Dragoni, D., Fischer, M. L., Flanagan, L. B., Grant, R., Gu, L., Hollinger, D., Izaurralde, R. C., Kucharik, C., Lafleur, P., Law, B. E., Li, L., Li, Z., Liu, S., Lokupitiya, E., Luo, Y., Ma, S., Margolis, H., Matamala, R., McCaughey, H., Monson, R. K., Oechel, W. C., Peng, C., Poulter, B., Price, D. T., Riciutto, D. M., Riley, W., Sahoo, A. K., Sprintsin, M., Sun, J., Tian, H., Tonitto, C., Verbeeck, H., and Verma, S. B.: A model-data intercomparison of CO_2 exchange across North America: Results from the North American Carbon Program site synthesis, Journal of Geophysical Research: Biogeosciences, 115, n/a-n/a, 2010.

Sellers, P. J., Bounoua, L., Collatz, G. J., Randall, D. A., Dazlich, D. A., Los, S. O., Berry, J. A., Fung, I., Tucker, C. J., Field, C. B., and Jensen, T. G.: Comparison of radiative and physiological effects of doubled atmospheric CO_2 on climate, Science, 271, 1402-1406, 1996.

Schädel, C, Schuur, E. A. G., Bracho R., Elberling, B., Knoblauch, C, Lee, H, Luo, Y.Q., Shaver, G. R., Turetsky, M. R. Circumpolar assessment of permafrost C quality and its vulnerability over time using long-term incubation data. Global Change Biology, **20**: 641–652, 2014.

Shi, Z., Yang, Y., Zhou, X., Weng, E., Finzi, A. C., and Luo, Y.: Inverse analysis of coupled carbon–nitrogen cycles against multiple datasets at ambient and elevated CO2, J Plant Ecol, 9, 285-295, 2016.

Sierra, C. A. and Müller, M.: A general mathematical framework for representing soil organic matter dynamics, Ecol Monogr, 85, 505-524, 2015.

Smith, J. U., Smith, P., Monaghan, R., and MacDonald, J.: When is a measured soil organic matter fraction equivalent to a model pool?, Eur J Soil Sci, 53, 405-416, 2002.

Smith, P., Davis, S. J., Creutzig, F., Fuss, S., Minx, J., Gabrielle, B., Kato, E., Jackson, R. B., Cowie, A., and Kriegler, E.: Biophysical and economic limits to negative CO_2 emissions, Nat Clim Change, 6, 42-50, 2016.

Stewart, C. E., Plante, A. F., Paustian, K., Conant, R. T., and Six, J.: Soil carbon saturation: Linking concept and measurable carbon pools, Soil Sci Soc Am J, 72, 379-392, 2008.

Thonicke, K., Spessa, A., Prentice, I., Harrison, S. P., Dong, L., and Carmona-Moreno, C.: The influence of vegetation, fire spread and fire behaviour on biomass burning and trace gas emissions: results from a process-based model, Biogeosciences, 7, 1991-2011, 2010.

Tian, H. Q., Yang, Q. C., Najjar, R. G., Ren, W., Friedrichs, M. A. M., Hopkinson, C. S., and Pan, S. F.: Anthropogenic and climatic influences on carbon fluxes from eastern North America

918   to the Atlantic Ocean: A process-based modeling study, J Geophys Res-Biogeo, 120, 752-772,
919   2015.

920   Todd-Brown, K. E. O., Randerson, J. T., Post, W. M., Hoffman, F. M., Tarnocai, C., Schuur, E.
921   A. G., and Allison, S. D.: Causes of variation in soil carbon simulations from CMIP5 Earth
922   system models and comparison with observations, Biogeosciences, 10, 1717-1736, 2013.

923   Walker, A. P., Aranda, I., Beckerman, A. P., Bown, H., Cernusak, L. A., Dang, Q. L.,
924   Domingues, T. F., Gu, L., Guo, S., Han, Q., Kattge, J., Kubiske, M., Manter, D., Merilo, E.,
925   Midgley, G., Porte, A., Scales, J. C., Tissue, D., Turnbull, T., Warren, C., Wohlfahrt, G.,
926   Woodward, F. I., and Wullschleger, S. D.: A Global Data Set of Leaf Photosynthetic Rates, Leaf
927   N and P, and Specific Leaf Area. Data set. Available on-line [http://daac.ornl.gov] from Oak
928   Ridge National Laboratory Distributed Active Archive Center, Oak Ridge, Tennessee, USA.
929   http://dx.doi.org/10.3334/ORNLDAAC/1224, 2014. 2014.

930   Wang, G. B., Zhou, Y., Xu, X., Ruan, H. H., and Wang, J. S.: Temperature Sensitivity of Soil
931   Organic Carbon Mineralization along an Elevation Gradient in the Wuyi Mountains, China, Plos
932   One, 8, 2013.

933   Wang, Y.-P. and Leuning, R.: A two-leaf model for canopy conductance, photosynthesis and
934   partitioning of available energy I:: Model description and comparison with a multi-layered
935   model, Agricultural and Forest Meteorology, 91, 89-111, 1998.

936   Wang, Y., Jiang, J., Chen-Charpentier, B., Agusto, F., Hastings, A., Hoffman, F., Rasmussen,
937   M., Smith, M., Todd-Brown, K., and Wang, Y.: Responses of two nonlinear microbial models to
938   warming and increased carbon input, Biogeosciences, 13, 887-902, 2016.

939   Wang, Y. P., Chen, B. C., Wieder, W. R., Leite, M., Medlyn, B. E., Rasmussen, M., Smith, M.
940   J., Agusto, F. B., Hoffman, F., and Luo, Y. Q.: Oscillatory behavior of two nonlinear microbial
941   models of soil carbon decomposition, Biogeosciences, 11, 1817-1831, 2014.

942   Weng, E. S. and Luo, Y. Q.: Soil hydrological properties regulate grassland ecosystem responses
943   to multifactor global change: A modeling analysis, J Geophys Res-Biogeo, 113, 2008.

944   Weng, E. S., Malyshev, S., Lichstein, J. W., Farrior, C. E., Dybzinski, R., Zhang, T.,
945   Shevliakova, E., and Pacala, S. W.: Scaling from individual trees to forests in an Earth system
946   modeling framework using a mathematically tractable model of height-structured competition,
947   Biogeosciences, 12, 2655-2694, 2015.

948   Weng, E. S. S., Luo, Y. Q., Wang, W. L., Wang, H., Hayes, D. J., McGuire, A. D., Hastings, A.,
949   and Schimel, D. S.: Ecosystem carbon storage capacity as affected by disturbance regimes: A
950   general theoretical model, J Geophys Res-Biogeo, 117, 2012.

951   West, T. O., Bandaru, V., Brandt, C. C., Schuh, A., and Ogle, S.: Regional uptake and release of
952   crop carbon in the United States, Biogeosciences, 8, 2037-2046, 2011.

953   Wieder, W. R., Bonan, G. B., and Allison, S. D.: Global soil carbon projections are improved by
954   modelling microbial processes, Nat Clim Change, 3, 909-912, 2013.

955 Xia, J. Y., Luo, Y. Q., Wang, Y. P., and Hararuk, O.: Traceable components of terrestrial carbon
956 storage capacity in biogeochemical models, Global Change Biol, 19, 2104-2116, 2013.

957 Xie, X. S.: Enzyme kinetics, past and present, Science, 342, 1457-1459, 2013.

958 Xu, X., Luo, Y. Q., and Zhou, J. Z.: Carbon quality and the temperature sensitivity of soil
959 organic carbon decomposition in a tallgrass prairie, Soil Biol Biochem, 50, 142-148, 2012.

960 Xu, X., Shi, Z., Li, D., Rey, A., Ruan, H. H., Craine, J. M., Liang, J., Zhou, J., and Luo, Y.: Soil
961 properties control decomposition of soil organic carbon: Results from data-assimilation analysis,
962 Geoderma, 262, 235-242, 2016.

963 Yang, Y. H., Luo, Y. Q., and Finzi, A. C.: Carbon and nitrogen dynamics during forest stand
964 development: a global synthesis, New Phytol, 190, 977-989, 2011.

965 Zhang, D. Q., Hui, D. F., Luo, Y. Q., and Zhou, G. Y.: Rates of litter decomposition in terrestrial
966 ecosystems: global patterns and controlling factors, J Plant Ecol, 1, 85-93, 2008.
967

968   **Fig. 1** The Terrestrial ECOsystem (TECO) model and its outputs. Panel a is a schematic

969   representation of C transfers among multiple pools in plant, litter and soil in the TECO model.

970   TECO has feedback loops of C among soil pools. CWD = coarse wood debris, SOM = Soil

971   Organic Matter. Panel b compares the original TECO model outputs with those from matrix

972   equations for net ecosystem production (NEP = the sum of elements in $X'(t)$ from eq. 1). The

973   perfect match between the TECO outputs and NEP from eq. 1 is due to the fact that they are

974   mathematically equivalent. Panel c compares the original TECO model outputs with those from

975   matrix equations for ecosystem C storage (= the sum of elements in $X(t)$ from eq. 2). The C

976   storage values calculated with eq. 2 are close to 1:1 line with r^2 =0.998 with the modeled values

977   (panel c). The minor mismatch in estimated C storage between the matrix equation calculation

978   and TECO outputs is due to numerical errors via inverse matrix operation with some small

979   numbers.

980

981   **Fig. 2** Seasonal cycles of the C storage capacity and C storage dynamics for the leaf pool (i.e.,

982   pool 1 as shown in Fig. 1). All the components are showed in panels b-d to calculate $x_{c,1}(t) =$

983    $b_1 u(t)\tau_1$ through multiplication, where $u(t) = NPP$ and $\tau_1 = 1/k_1$ for leaf.

984

985   **Fig. 3** Seasonal cycles of the C storage capacity and C storage dynamics for the litter pool (i.e.,

986   pool 4 as shown in Fig. 1). All the components are showed to calculate

987    $x_{c,4,u}(t) = \sum_{j=1}^{n} f_{4j} \tau_4 b_j u(t)$ in panels b-e and $x_{c,4,p}(t) = \sum_{j=1,j\neq 4}^{n} f_{4j} \tau_4 x'_j(t)$ in panels f-i for

988   litter. $x_{c,4,u}(t)$ is the maximal amount of C that can transfer from C input to the litter pool.

989    $x_{c,4,p}(t)$ is the maximal amount of C that can transfer from all the other pools to the litter pool.

990   This figure is to illustrate the network of pools through which C is distributed.

991

Fig. 4 Components of the C storage capacity for litter pool (i.e., pool 4 as shown in Fig. 1).

Component, $x_{c,4,u}(t)$, is the C from C input and component, $x_{c,4,p}(t)$, is the C from all the other

pools to the litter pool. The sum of them is the attractor that determines the direction of C storage

change in pool 4.

996

Fig. 5 Transient dynamics of ecosystem C storage in response to global change in Harvard

Forest. Panel a shows the time courses of the ecosystem C storage capacity, the ecosystem C

storage potential, and ecosystem C storage (i.e., C stock) from 1850 to 2100. Panel b shows time

courses of NPP(t) as C input and ecosystem residence times. Panel c shows correlated changes in

ecosystem C storage potential and net ecosystem production (NEP). Panel d illustrates the
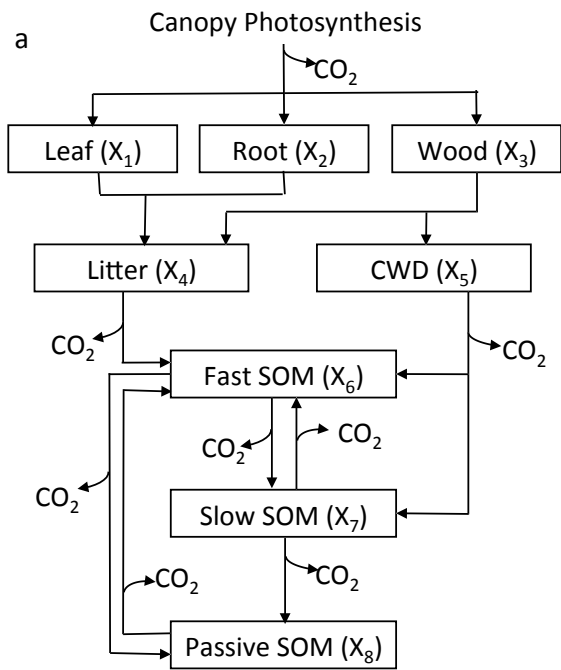
regression between the C storage potential and NEP.

1003

Fig. 6 The C storage capacity ($x_{c,i}(t)$), the C storage potential ($x_{p,i}(t)$), and C storage ($x_i(t)$) of

individual pools. The potential is nearly zero for those fast turnover pools with short residence

times but very large for those pools with long residence times.

1007

Fig. 7 The C storage potential of individual pools ($x_{p,i}$) as influenced by net C pool change of

different pools (x'_i) in their corresponding rows. The correlation coefficients show the degree of

influences of net C pool change in one pool on the C storage potential of the corresponding pool

through the network of C transfer. Those empty cells indicate no pathways of C transfer between
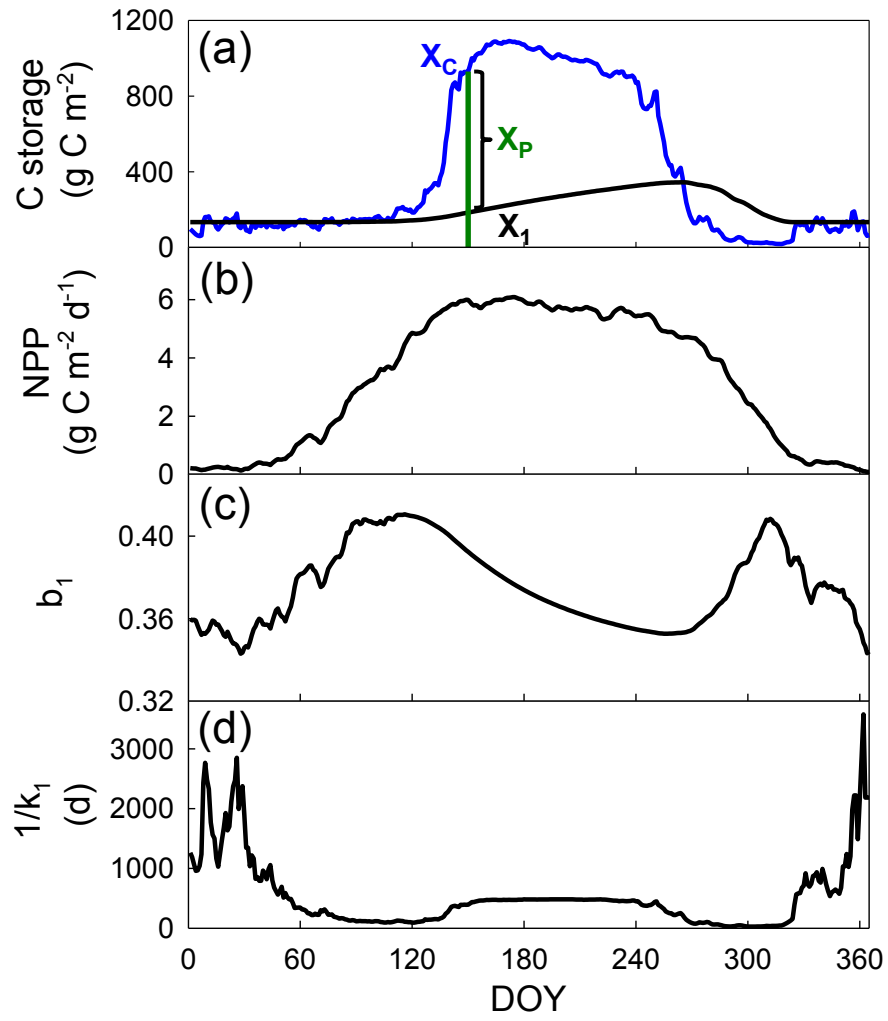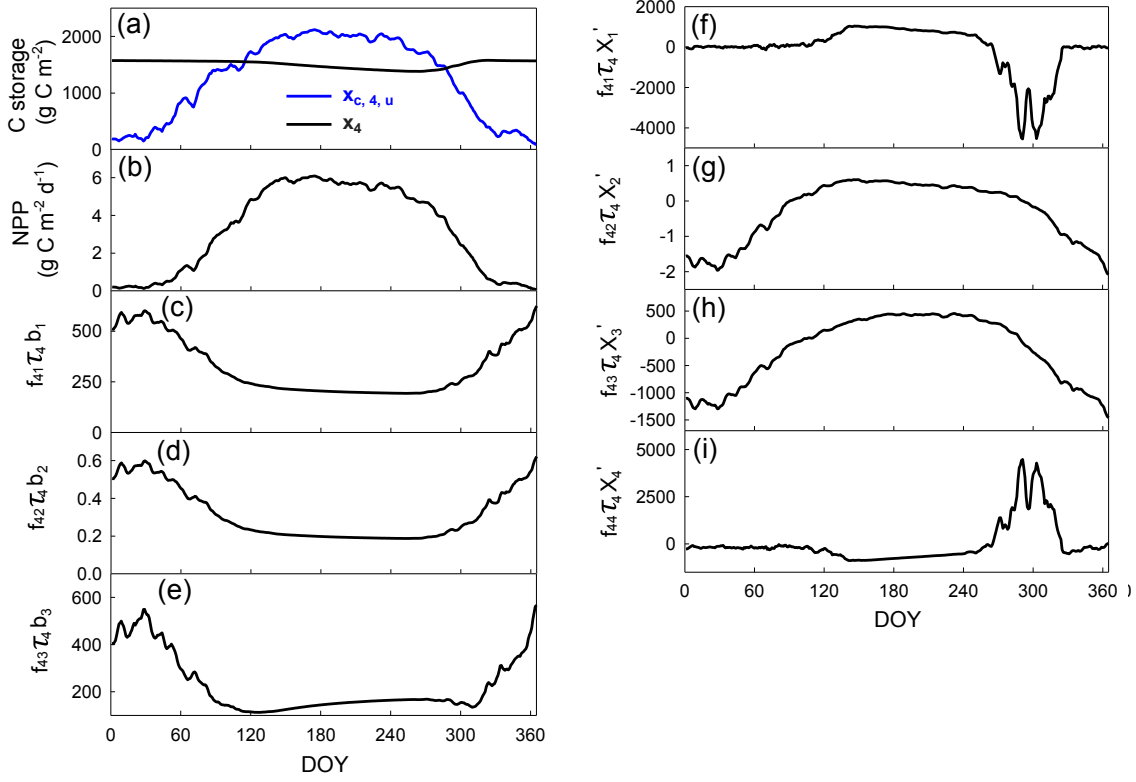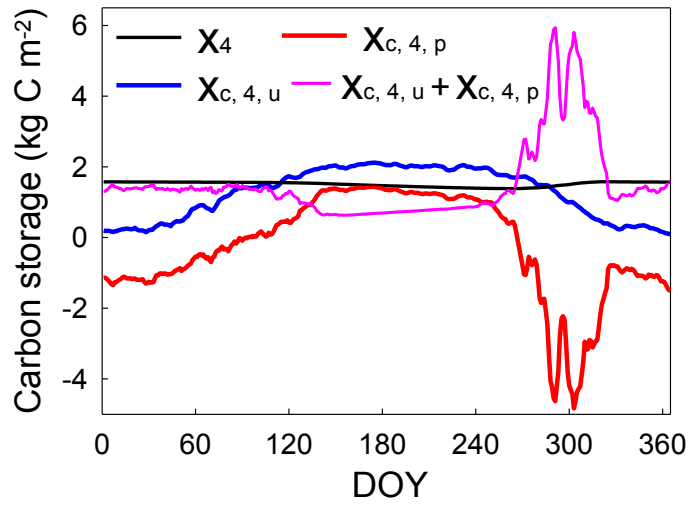
those pools as indicated in Fig. 1.

1013

a

Canopy Photosynthesis

CO_2

Leaf (X_1) Root (X_2) Wood (X_3)

Litter (X_4) CWD (X_5)

CO_2 CO_2

Fast SOM (X_6)

CO_2 CO_2

CO_2

Slow SOM (X_7)

CO_2 CO_2

Passive SOM (X_8)

b

1:1 line

c

1:1 line

Fig. 1

1014
1015
1016

b: y-axis "NEE from matrix equation (g C m⁻² d⁻¹)", x-axis "NEE from TECO output (g C m⁻² d⁻¹)"

c: y-axis "X from matrix equation (kg C m⁻²)", x-axis "X from TECO output (kg C m⁻²)"
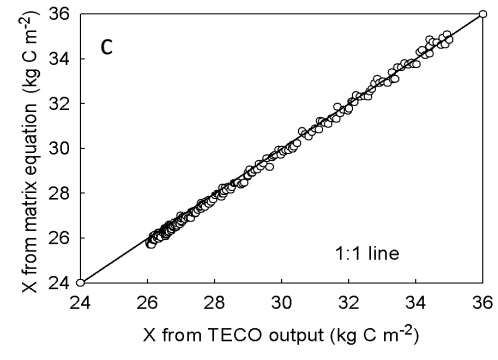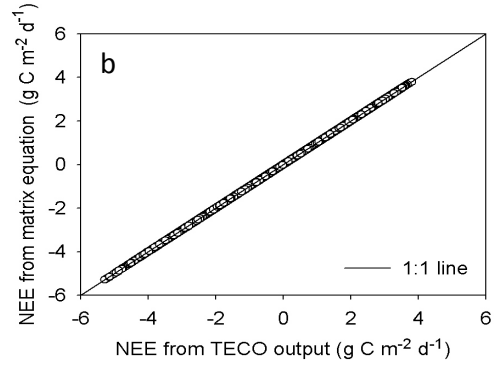
Fig. 2

1017
1018
1019
1020
1021
1022

Fig. 3

1025
1026

1027
1028
1029   Fig. 4

1030

1031
1032
1033　　　　　　　　　Fig. 5
1034
1035

1036
1037
1038   Fig. 6
1039

Fig. 7